On the Mixing Coefficient in the Parameterization of Bolus Velocity

KIRK BRYAN

Program in Atmospheric and Oceanic Sciences, Princeton University, Princeton, New Jersey

JOHN K. DUKOWICZ AND RICHARD D. SMITH

Theoretical Division, Los Alamos National Laboratory, Los Alamos, New Mexico

ABSTRACT

Mesoscale eddies in the ocean play an important role in the ocean circulation. In order to simulate the ocean circulation, mesoscale eddies must be included explicitly or parameterized. The eddy permitting calculations of the Los Alamos ocean circulation model offer a special opportunity to test aspects of parameterizations that have recently been proposed. Although the calculations are for a model in level coordinates, averages over a five-year period have been carried out by interpolating to instantaneous isopycnal surfaces. The magnitude of "thickness mixing" or bolus velocity is found to coincide with areas of intense mesoscale activity in the western boundary currents of the Northern Hemisphere and the Antarctic Circumpolar Current. The model also predicts relatively large bolus fluxes in the equatorial region. The analysis does show that the rotational component of the bolus velocity is significant. Predictions of the magnitude of the bolus velocity, assuming downgradient mixing of thickness with various mixing coefficients, have been compared directly with the model. The coefficient proposed by Held and Larichev provides a rather poor fit to the model results because it predicts large bolus velocity magnitudes at high latitudes and in other areas in which there is only a small amount of mesoscale activity. A much better fit is obtained using a constant mixing coefficient or a mixing coefficient originally proposed by Stone in a somewhat different context. The best fit to the model is obtained with a coefficient proportional to λ^2/T, where λ is the radius of deformation, and T is the Eady timescale for the growth of unstable baroclinic waves.

1. Introduction

Satellite observations and high-resolution numerical models provide an unparalleled global picture of mesoscale eddies in the World Ocean (Fu and Smith 1996). In spite of new global satellite data on the energy distribution of mesoscale eddies, their actual role in the ocean circulation is still not fully understood. The long-term, in situ, measurements required to directly measure the momentum and heat transfer by mesoscale eddies have only been made for a few sites, and cannot be considered representative for the whole globe. Mesoscale eddies are directly analogous to synoptic scale disturbances in the atmosphere. Many ideas that have been developed in studying atmospheric dynamics may also apply to mesoscale eddies, but there are important differences (Rhines 1975). For example, the ocean is broken up into basins separated by barriers so that the World Ocean lacks the zonal symmetry of the atmosphere.

A remarkable feature of the ocean circulation is that, in spite of the existence of energetic mesoscale eddies, ocean atlases show that water mass properties are conserved along trajectories of thousands of kilometers (Reid and Lynn 1971), which require decades to traverse by deep western boundary currents. This feature makes the ocean very different from the atmosphere, where air mass properties are conserved only for a day or two. Mesoscale eddies apparently stir the ocean in such a way that the trajectories of water parcels conserve water mass properties to a large degree. Stated in another way, the trajectories associated with mesoscale eddies are nearly parallel to density surfaces and will therefore cause lateral spreading, but will not cause vertical mixing within the water column. As an example, consider unstable mesoscale eddies on an ocean front with strongly sloping isopycnal surfaces. The unstable mesoscale eddies tend to flatten the isopycnal surfaces across the front without mixing of density across isopycnal surfaces. This does not mean that mesoscale eddies in the ocean are fundamentally different from synoptic-scale disturbances in the atmosphere. The differ-

Corresponding author address: Dr. Kirk Bryan, Program in Atmospheric and Oceanic Sciences, Princeton University, Post Office Box CN710, Sayre Hall, Princeton, NJ 08544-0710.
E-mail: kbryan@splash.princeton.edu

ence is that below the mixed layer, mesoscale eddies in the ocean exist in an environment relatively free of small-scale sources and sinks of buoyancy.

Gent and McWilliams (1990, hereafter GM) have initiated a very important debate on how mesoscale eddies affect the ocean circulation. This debate has purely practical implications in the design of coupled models for climate research, as well as scientific implications for a better understanding of the role of quasigeostrophic turbulence in the ocean. As Gent and McWilliams point out, the traditional representation of mesoscale eddies in level-coordinate ocean general circulation models as a purely diffusive process in the horizontal plane does not conserve density and so is clearly an inadequate representation. In this respect ocean circulation models of low horizontal resolution using an isopycnal vertical coordinate have a clear advantage. In isopycnal models it is relatively easy to introduce the GM parameterization to mix tracers and layer thickness along isopycnal surfaces, simulating the effects of mesoscale eddies that conserve density. In an attempt to introduce a more accurate parameterization of the adiabatic mixing by mesoscale eddies into coarse resolution, z-coordinate models, Redi (1982) and Cox (1987) introduced a mixing tensor for ocean circulation models that would mix tracers along isopycnal surfaces rather than horizontal surfaces. GM have introduced a more general parameterization for level-coordinate models that includes the Redi–Cox scheme, but also represents the mixing of vertical stability gradients by mesoscale eddies. This was a very important step because the dynamic effects of mesoscale eddies, such as the flattening of fronts, were then included. This scheme allows for the destruction of available potential energy without mixing across density surfaces. Danabasoglu et al. (1994) and Böning et al. (1995) have shown that the use of the GM scheme appears to greatly improve the performance of level-coordinate ocean circulation models of low and intermediate resolution. An important aspect of the GM scheme is to eliminate the Veronis (1975) effect in which horizontal mixing causes mixing across density surfaces. As far as can be determined from limited observational data, poleward heat transport is better simulated by models with the GM parameterization, which is a very important feature for climate research.

The physical idea behind the GM model is that mesoscale eddies in the ocean would tend to reduce available potential energy and that this process can be approximated as "thickness mixing" down the thickness gradient. The GM mixing is a purely adiabatic process, reducing the available potential energy and removing differences of stratification. GM derive their parameterization by considering averages with respect to density in an isopycnal model. If the mixing coefficient is independent of z, their thickness flux is proportional to the gradient of thickness, and appears in the continuity equation as

$$\nabla_\rho \cdot (\overline{\mathbf{u}'h'}) = \nabla_\rho \cdot (\mathbf{u}_b\overline{h}) = -\nabla_\rho \cdot (K\nabla_\rho\overline{h}). \quad (1)$$

Therefore, the bolus velocity, $\mathbf{u}_b$, can be expressed in general as

$$\mathbf{u}_b = -\frac{K}{\overline{h}}\nabla_\rho\overline{h} + \text{a rotational component.} \quad (2)$$

Here ∇_ρ is the gradient parallel to density surfaces, and $h = -\rho_0 z_\rho$. An overbar indicates an ensemble average on a density surface, which is evaluated as a time average in this study. The original GM parameterization adds a bolus velocity term wherever the mean velocity appears in the time averaged continuity and tracer equations. While the GM parameterization makes the important contribution of improving level-coordinate models, questions still remain as to the details. The exact form of the closure is left open, but GM suggest that the simplest form of the parameterization with a downgradient mixing of thickness with a uniform mixing coefficient might be sufficient to represent the effect of unstable mesoscale eddies on the ocean circulation in low resolution models.

Held and Larichev (1996, hereafter HL) suggest that the GM parameterization would be improved if a spatially nonuniform mixing coefficient were introduced. On the basis of some idealized simulations of geostrophic turbulence, they suggest a specific expression for the mixing coefficient of GM. Visbeck et al. (1997, hereafter VMHS) have also explored nonconstant mixing coefficients. They carried out three quite different three-dimensional, eddy-resolving simulations of ocean flows, and then attempted to fit the solutions to much simpler two-dimensional models with parameterizations of the mesoscale eddies. Their study suggested that the best fit could be obtained with a mesoscale eddy mixing based on the suggestions of Green (1970) and Stone (1972). Treguier et al. (1997) show that the global observations of the variance of surface topography coincide to a certain extent with a large-scale inverse Richardson number, which also supports the type of nonuniform mixing coefficient advocated by HL and VMHS.

A precedent for using an eddy resolving ocean circulation model to study bolus flows has been established in a pioneering study by Rix and Willebrand (1996). Their study is based on North Atlantic model calculations carried out by Böning and Hermann (1994), which were part of the WOCE Community Modeling Effort. The Rix and Willebrand analysis provides a detailed comparison of model results with the closure proposed by GM for a 4000 km by 2000 km region of the model in the eastern part of the North Atlantic subtropical gyre. Although the mesoscale eddies were relatively weak in this region, the radius of deformation was large enough for eddy scales to be well resolved by the numerical model. Rix and Willebrand suggested that the averaging period of 20 years was too short to allow examination of spatial variations of a thickness

TABLE 1. Horizontal resolution of the POP Global Ocean circulation model as well as zonal averages of the first-mode radius of deformation, $\sqrt{C_1}f^{-1}$, and the analyzed eddy length scale from Fig. 1 and Fig. 26 of Maltrud et al. (1998). C_1 is the speed of a gravity wave of mode one.

	Latitude (deg)						
	10	20	30	40	50	60	70
	Grid size (km)						
	30.8	29.4	26.0	23.9	20.1	15.6	10.7
Northern Hemisphere							
First-mode radius (km)	>100	60	37	24	14	5	2
Eddy scale (km)	170	120	100	80	70	65	80
Southern Hemisphere							
First-mode radius (km)	>100	55	38	20	16	9	2
Eddy scale (km)	185	130	110	90	70	60	80

diffusion coefficient, or allow a study of areas in the model with more intense mesoscale activity.

The goal of the present study is to examine some of these issues using a five year archive of the Los Alamos Parallel Ocean Program (POP) ocean circulation model (Fu and Smith 1996; Maltrud et al. 1998). Although this is perhaps the most detailed global model study published up to this time, it must be recognized that it is still far from ideal for a study of this kind. It is a *z*-coordinate model in which the lateral diffusion across density surfaces is minimized by high resolution and biharmonic diffusion, but is still present. The model permits a highly energetic mesoscale eddy field, but it cannot fully resolve eddies, particularly at high latitudes. The treatment of topography is somewhat crude because of the discretization of the total depth into fixed intervals. The global model is spun up from initial conditions based on Levitus (1982) data in a series of integrations. The details of the spinup procedure and vertical resolution are given in an appendix at the end of this note. Table 1 provides an idea of the grid spacing, the radius of deformation and the eddy length scales in the model as computed by Maltrud et al. (1998). The model is based on a Mercator projection so that the east–west and north–south resolution are equal at all latitudes. The domain extends from 77°S to 77°N latitude. Table 1 shows that the resolution is about 30 km near the equator decreasing to a little over 10 km at 70° latitude. The grid spacing is less than the radius of deformation equatorward of 40° latitude in both hemispheres, but is almost twice the radius of deformation poleward of 60°. The eddy length scale estimated by Maltrud et al. (1998) is about 3–4 times the first-mode radius of deformation where the radius of deformation is well resolved, but asymptotes to a nearly constant value at higher latitudes where the resolution is poorer. Clearly much higher resolution models are needed for accurate simulation of mesoscale activity at higher latitudes.

The archived data have the disadvantage of being a rather short sample in time. As pointed out by Rix and Willebrand (1996) baroclinic instability is a chaotic pro-

cess so that stable averages are difficult to obtain without a very long record. Perhaps an even more important factor, which is not fully taken into account in their study, is the existence of a strong rotational component of the bolus flux. There is no reason to expect that a time average over a very long period would remove the rotational component. In our analysis we have found that rotational and divergent components of the bolus velocity are of similar magnitude and are both concentrated in areas of intense mesoscale activity. Ideally it would be desirable to separate bolus velocities into a rotational and divergent component. However, the boundary conditions on density surfaces for making such a decomposition are problematical and prevent such a separation. Instead, we have used two measures for the purpose of a global comparison with parameterizations. 1) The scalar bolus velocity, which is the smoothed magnitude of the bolus velocity, is employed in section 3. This has the advantage of being directly related to the bolus flux, but it has the disadvantage of lumping together the divergent and rotational components. 2) The smoothed absolute value of the divergence of the bolus flux which is employed in section 4. This measure has the advantage that it eliminates the contribution of the rotational component, but it has the disadvantage that it is only indirectly related to the bolus flux. However, these measures are found to be strongly correlated in spite of their differences, and both give similar and supporting results.

Tests showed that projecting level-coordinate averages onto time-averaged density surfaces produced large flows normal to the time-averaged density surfaces in regions of the ocean with low vertical stability. This effect has also been noted by McDougall and McIntosh (1996). For this reason the model data, which were calculated originally in a fixed level-coordinate system, have been time-averaged on density surfaces as the integration proceeds. The global domain of the model is important. The results permit a global view of the role of mesoscale eddies in the World Ocean within the limitations of the model resolution. It allows baroclinic processes in separate high mesoscale energy regions in the Northern and Southern Hemispheres to be compared. Ideally, a parameterization of mesoscale eddies should work equally well in all parts of the World Ocean.

The next section is a statistical analysis of some of the properties of ''thickness mixing'' in the POP model on a single density surface. In section 3 the global distributions of the magnitude of the bolus velocities associated with thickness mixing are examined. The variables are based on averages on density surfaces, but interpolated to 150 and 300 m. The bolus data from the model are compared with the predictions of three different parameterization schemes. A summary and conclusions based on the analysis are presented in the final section.

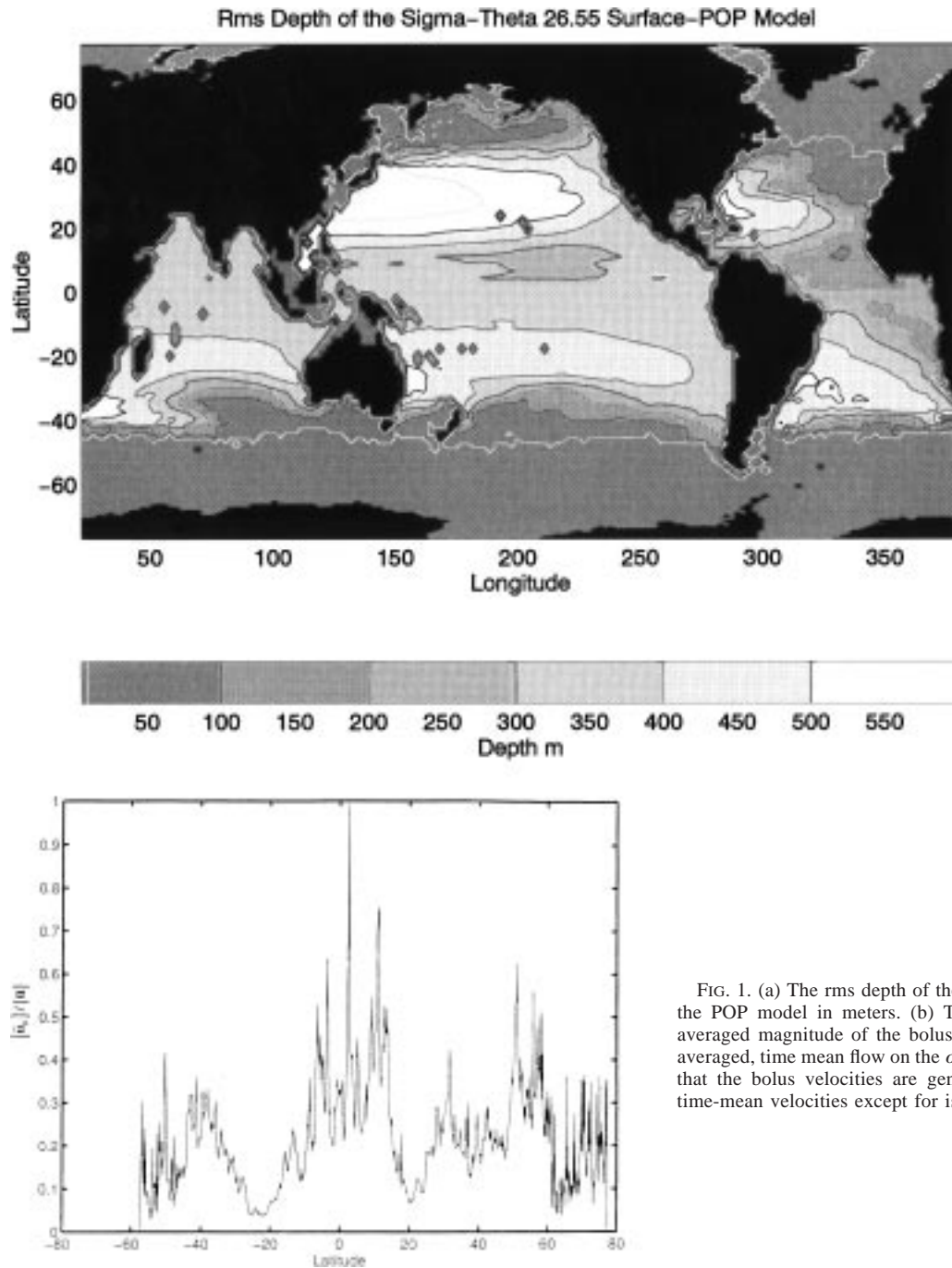Rms Depth of the Sigma–Theta 26.55 Surface–POP Model

FIG. 1. (a) The rms depth of the $\sigma_\Theta = 26.55$ surface of the POP model in meters. (b) The ratio of the zonally averaged magnitude of the bolus velocity to the zonally averaged, time mean flow on the $\sigma_\Theta = 26.55$ surface. Note that the bolus velocities are generally smaller than the time-mean velocities except for isolated peaks.

2. Analysis of the POP statistics on a constant density surface

During the last five years of Stage III of the POP run (see appendix) the variables were saved at intervals of 10 days so that an averaging on isopycnal surfaces could be carried out. All the results in this paper will be based on these isopycnal averages for this final five-year period. Averages were carried out on potential density surfaces referenced to surface pressure, or σ_Θ surfaces.

The bolus velocity was calculated by making averages of velocity, thickness, and the product of velocity and thickness on 40 instantaneous σ_Θ surfaces, which were spaced 0.1 σ_Θ unit apart. The bolus velocity as defined in (1) is calculated from

$$\overline{h}\mathbf{u}_b = \overline{\mathbf{u}\overline{h}} - \overline{\mathbf{u}}\,\overline{h}. \tag{3}$$

Before actually testing parameterization schemes, it is important to describe the basic statistics of thickness
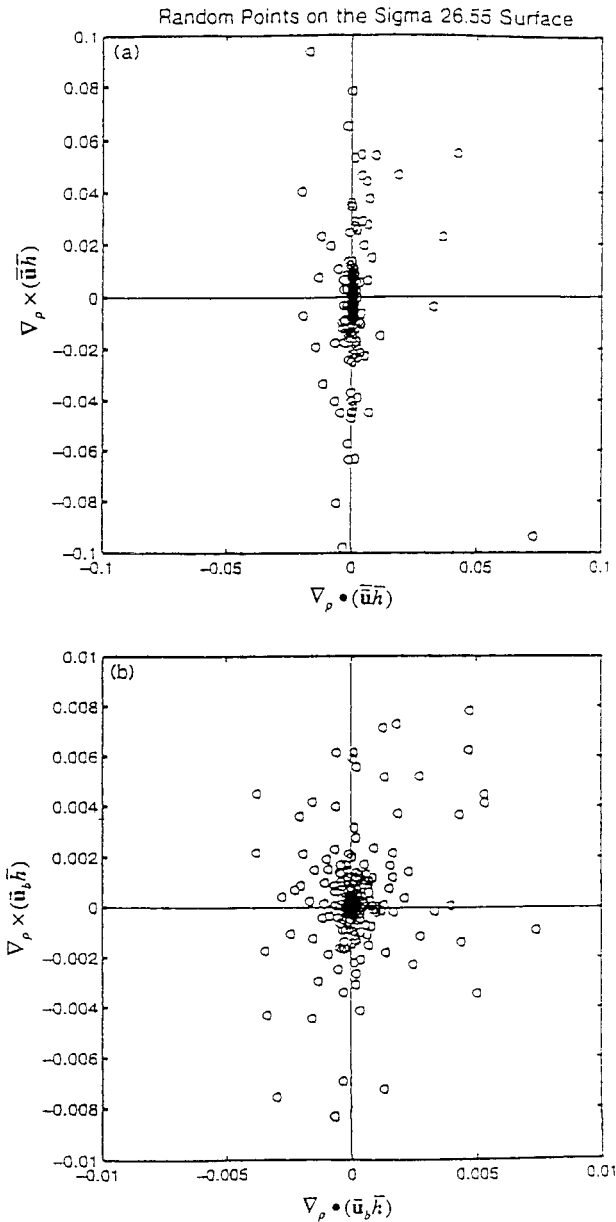
Random Points on the Sigma 26.55 Surface

FIG. 2. (a) Curl vs divergence of thickness flux due to the time-mean flow. A scatter diagram of random points with respect to area on the $\sigma_\Theta = 26.55$ surface. (b) The same for the thickness flux due to eddies. Note the difference in scale. Also note the curl of the thickness flux is roughly equal or larger than the divergence. The divergence of the thickness flux is in units of 100 m s^{-1}.

mixing by mesoscale eddies in the POP model. We will concentrate in this section on the $\sigma_\Theta = 26.55$ surface as a representative surface in the upper thermocline. The rms depth of this surface is shown in Fig. 1a. Note that the surface outcrops poleward of 40°N and 40°S. The region of the Antarctic Circumpolar Current is not included, but the areas of intense mesoscale activity in the western boundary currents are. Table 1 shows that the resolution of the model is adequate to resolve the

first-mode radius of deformation in the region covered by this density surface. The surface only extends to 400–500 m depth in the Atlantic, but is about 100 m deeper in the North Pacific. In Fig. 1b the zonally averaged magnitude of the bolus velocity, divided by the magnitude of the zonally averaged, time-mean velocity, is shown as a function of latitude. The ratio is generally between 0.1 and 0.5, with isolated peaks rising to unity.

In Fig. 2a the curl of the thickness flux due to the time-averaged flow (the product of the mean velocity and the mean thickness) is compared with the divergence of thickness flux. As expected for flow strongly constrained by rotation, the curl of the time-averaged flow appears to be larger than the divergence. Figure 2b shows the same relationship for the bolus fluxes on the same $\sigma_\Theta = 26.55$ surface. It is evident that the bolus flux has a rotational component that may be equal to, if not larger than, the divergent component. It is clear that the bolus velocity is more than just an agent of thickness mixing, and flows are set up that are not closely linked to thickness source or sinks. It is not surprising that thickness fluxes should have a significant rotational component (Lau and Wallace 1979; Marshall and Shutts 1981). A concrete example of this type of flux is the case of nearly solitary mesoscale eddies observed in the ocean. They carry with them a positive thickness anomaly and may not be directly associated with significant thickness gradients. As pointed out in the introduction, it is clear that a rotational component of the bolus flux should be expected, and there is no reason to expect it to disappear with averaging over extended time periods.

3. Analysis of the amplitude of thickness mixing on constant-*z* surfaces

We now turn to statistics in which the averages determined on density surfaces are interpolated to horizontal surfaces at depths 150 m and 300 m. This representation has the advantage of presenting a global view of the patterns not interrupted by outcrop boundaries. The linear interpolation from the 40 density surfaces is reasonably accurate for all points except those in extreme polar waters where only a few density surfaces are represented in the water column. In all the figures that follow, fields are smoothed in the horizontal plane by minimizing the following integral:

$$I = \int\int \left((\boldsymbol{\nabla}\alpha)^2 + \frac{1}{\gamma^2}(\alpha - \hat{\alpha})^2 \right) dA, \qquad (4)$$

where α is the field to be smoothed, $\hat{\alpha}$ is the original field, and γ is the smoothing space scale, which is taken to be 500 km. Minimizing (4) is equivalent to solving a smoothing least squares problem. Ideally one would like to break the bolus velocity down into a rotational and a divergent component. However, we have not found this to be practical on the complicated geometry of the isopycnal surfaces. Figure 3 illustrates the dif-
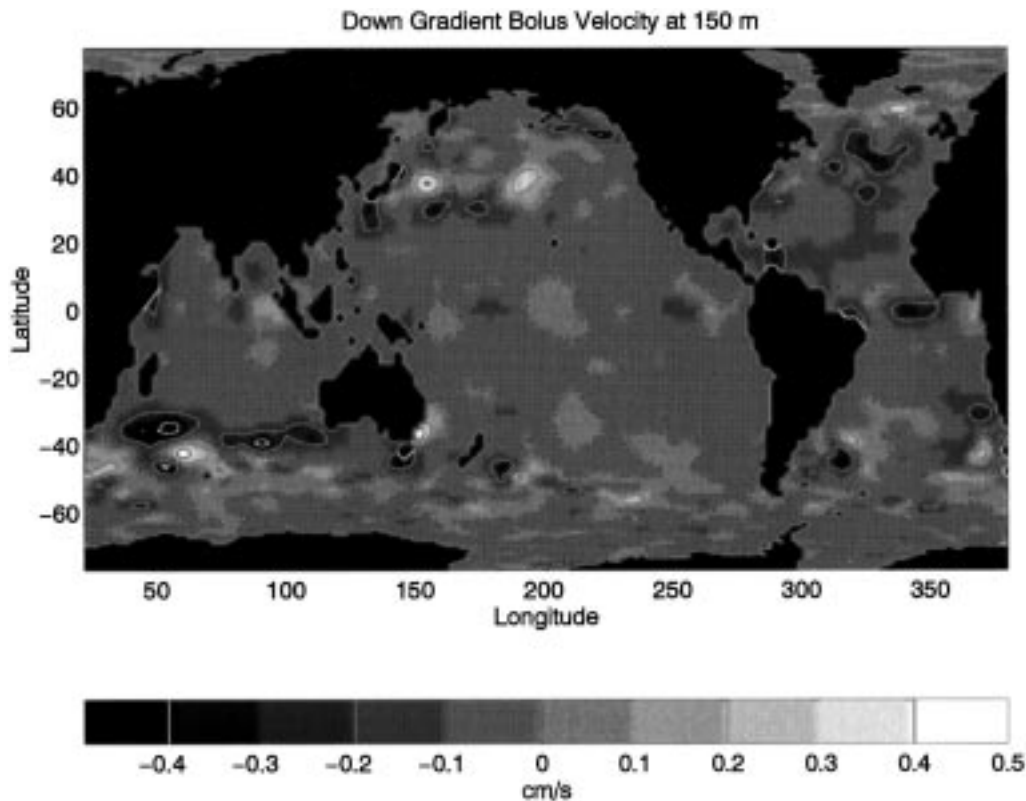
FIG. 3. The average magnitude of the bolus velocity parallel to the gradient of thickness on isopycnal surfaces, but projected onto the 150-m level. This quantity is positive for a bolus flux down the thickness gradient. The units are cm s^{-1}.

ficulties of a naive view of the bolus velocity field, which does not take into account the rotational component. In this figure we have interpolated the bolus velocity, which is based on averages on instantaneous density surfaces, to a level surface at 150 m, and then projected it parallel to the thickness gradient. The sign is taken so that bolus flux down the thickness gradient is positive. If there were no rotational bolus component and the formation of mesoscale eddies were a purely local process, we would expect to see only positive regions concentrated around the major currents of the World Ocean. Instead a much more complicated picture emerges. There are both positive and negative regions, and the relationship to currents does not follow any simple rule. We see a weak positive area in the Gulf Stream region and in the outflow of the Brazil Current. In general, however, the pattern in Fig. 3 shows that a direct, local evaluation of a mixing coefficient for the GM parameterization in high energy areas is not feasible if the rotational component of the velocity field is not removed. Instead, we are forced to use a much more indirect approach using lumped statistics and a partially qualitative comparison of global patterns.

The magnitude of the bolus velocity in the POP model without regard to direction is shown in Figs. 4a and 4b. The global pattern at 150 m shows strong bolus flows in regions where vigorous mesoscale eddy activity is expected, such as the western boundary currents of the Northern Hemisphere oceans and the Circumpolar Current. However, there are also local maxima at the equator in both the eastern Atlantic and eastern Pacific. The smoothing specified by (4) reduces maximum values so that regions of strong eddy energy have bolus velocities of only 1–2 cm s^{-1}. The intensity is less at 300 m compared with 150 m, and this difference is largest along the equator where the thermocline is particularly shallow. The weaker amplitude at 300 m as compared to 150 m shows why it is better to view the bolus velocity at a level surface rather than on a density surface. The depth of a density surface varies so much that the patterns of bolus velocity on a density surface are mainly a function of the depth of the surface.

The predicted pattern of the magnitude of the bolus velocity based on the simplest GM closure as defined in (2) is shown in Fig. 5. A fixed constant of $K = 1000$ m^2 s^{-1} was used. The gradients of thickness on the isopycnal layers, which are averaged for the 5-yr time series, are interpolated on to the 150-m level. To evaluate the parameterization, the pattern can be compared to the model simulated bolus field of Fig. 4a. The global constant could be adjusted to give a better fit to Fig. 4a, but the most interesting result is the qualitative differ-
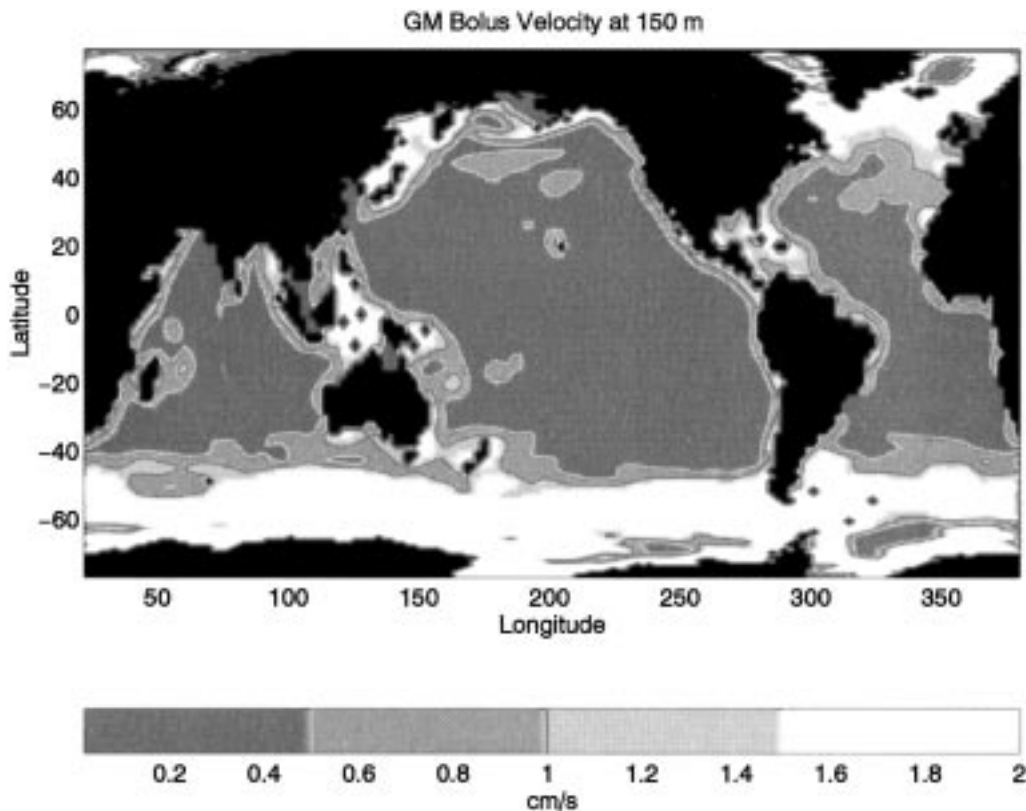
Bolus Velocity at 150 m

Bolus Velocity at 300 m
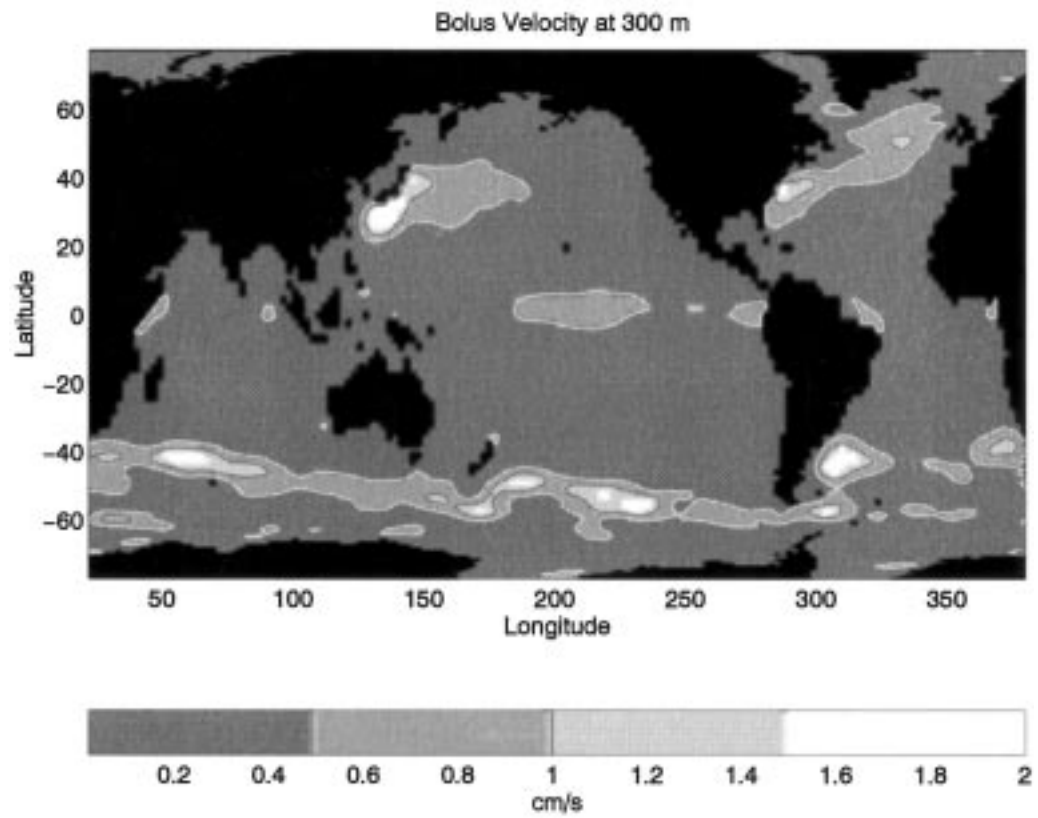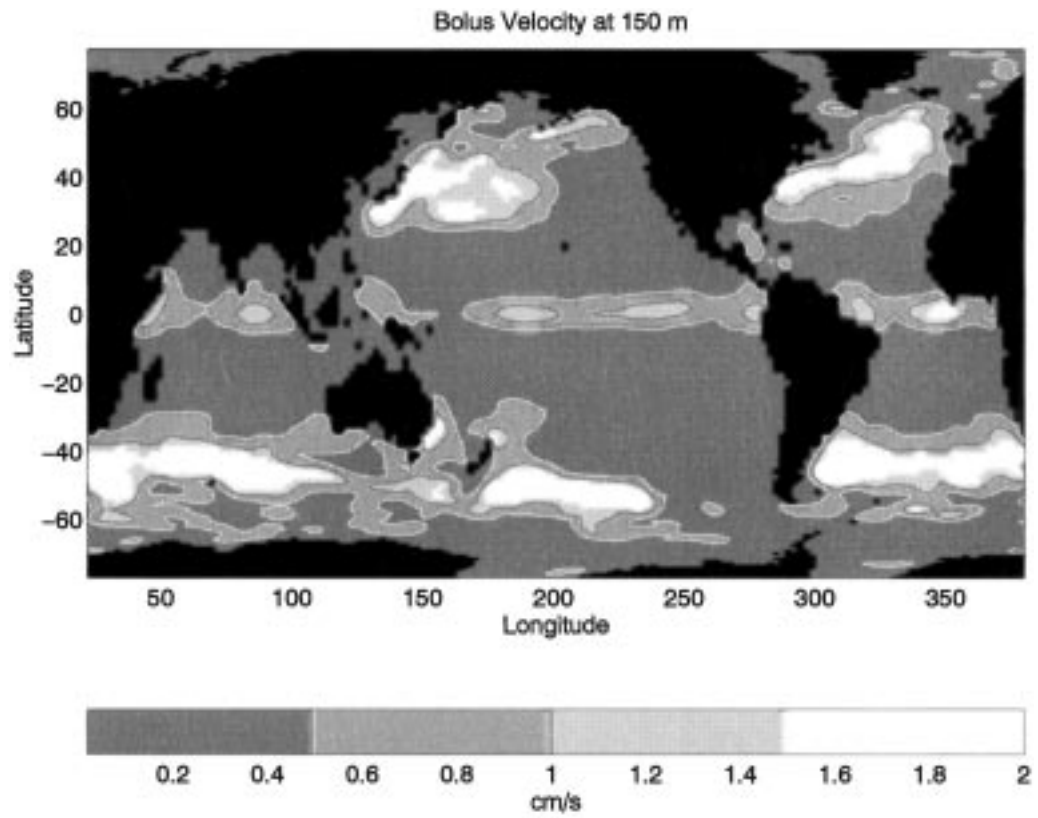
FIG. 5. The bolus velocity predicted by the Gent–McWilliams simple closure, at the 150-m level, using a mixing coefficient of 1000 m² s⁻¹.

ence in the predicted bolus velocity patterns of Fig. 4a and Fig. 5. In particular, this simple closure predicts very high bolus velocities in polar areas of weak vertical stratification and almost no bolus velocity amplitude in the Tropics. This is very different from the bolus velocities in the model simulation, which have local maxima at the equator and almost no bolus activity at very high latitudes. The tendency to predict bolus amplitude along the edge of continents, almost everywhere, is partly an artifact of the smoothing. An examination of the unsmoothed fields shows local blobs of high thickness gradient along the edges of the continents. The smoothing transforms these local blobs into strips of high amplitude parallel to the coasts. One concern is that very large slopes of isopycnals may be responsible for the poor fit to the POP model in high-latitude regions. Recently, Danabasoglu and McWilliams (1995) have introduced a taper in the GM closure scheme to reduce bolus flow in regions of large slope. As a test, their taper was calculated for the slopes of the POP model projected onto the 150- and 300-m surfaces (not shown). The taper

is nearly unity over the entire World Ocean in the model, indicating that it would have a negligible effect in reducing the high bolus velocities predicted for high latitudes shown in Fig. 5.

The suggestion that a nonuniform mixing coefficient might be more appropriate for representing geostrophic turbulence goes back to studies by Green (1970) and Stone (1972) for the atmosphere. For purposes of discussion the mixing coefficient can be represented by

$$K = L^2/T, \qquad (5)$$

where L is a mixing length scale, and T is an appropriate timescale. HL followed these early studies in selecting the timescale T to be the Eady (1949) timescale for the growth of unstable baroclinic disturbances:

$$\text{Eady timescale} = T = \frac{\sqrt{\text{Ri}}}{f}. \qquad (6)$$

The Richardson number is defined as $\text{Ri} = N^2/(\partial_z \mathbf{u})^2$, where N is the bouyancy frequency, $N = \sqrt{-\rho_0^{-1}g\partial_z\rho}$.

←

FIG. 4. The magnitude of the bolus velocity determined from averaging on isopycnal surfaces for the POP model are plotted on constant z surfaces at (a) the 150-m level and (b) the 300-m level.
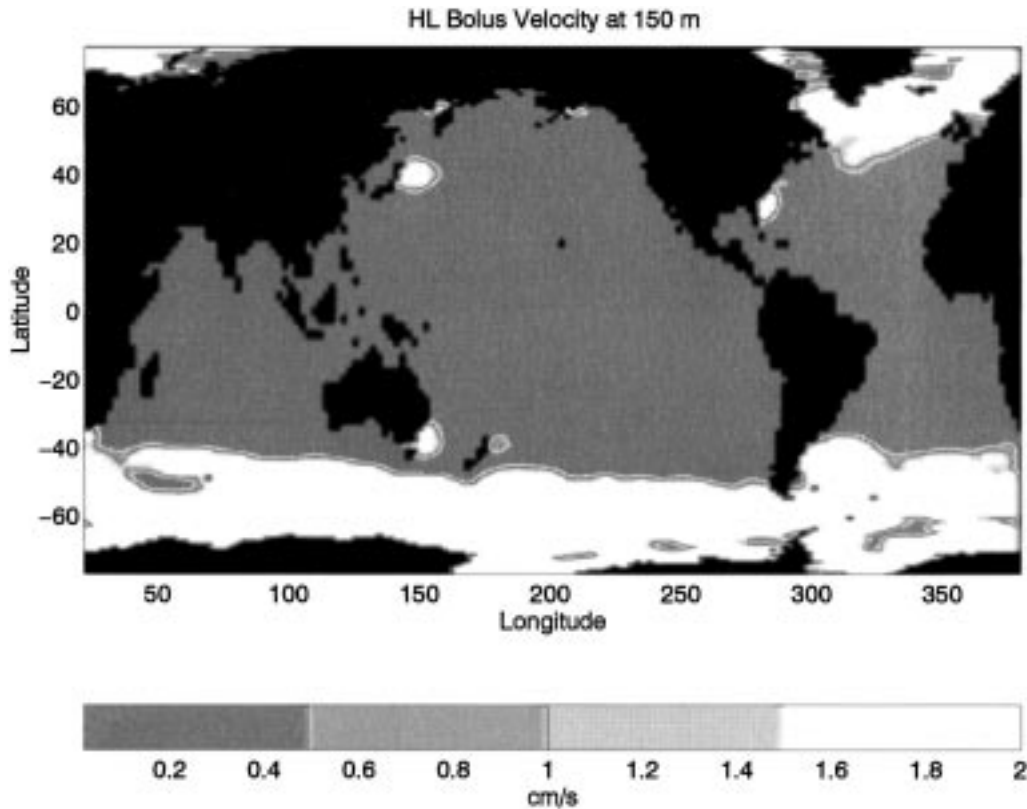
Fɪɢ. 6. The bolus velocities predicted by the Held–Larichev diffusion coefficient (with a factor of 0.001) at the 150-m level.

Treguier et al. (1997) have calculated the Eady timescale based on hydrographic data from the Levitus (1982) atlas. They find that the inverse timescale shows a reasonable correspondence to areas of high mesoscale energy as observed by satellite altimetry. For a space scale, HL have used a property of geostrophic turbulence pointed out by Rhines (1975). In geostrophic turbulence space scales will expand by inverse energy cascade until interrupted by dispersion through the beta effect. The Rhines (1975) scale is

$$L_R = \sqrt{\frac{U}{\beta}}. \tag{7}$$

Assuming $U = L_R/T$ in (7), HL obtain a mixing coefficient of the form

$$K_{\mathrm{HL}} = \frac{1}{\beta^2 T^3}. \tag{8}$$

The beta effect need not be due to the usual planetary beta, but it could also be due to bottom topography. The "effective beta," β_e, due to bottom topography, is defined by

$$\beta_e \equiv D\boldsymbol{\nabla}(f/D), \tag{9}$$

where D is the depth. Note that the mixing coefficient in (8) depends on the inverse $\frac{3}{2}$ power of the Richardson

number, which makes the mixing coefficient very large in areas of large shears of the time-averaged velocity. In applying this scaling to the statistics of the POP model it was found that the Eady timescale is only about one day for many high energy areas. Treguier et al. (1997) found an Eady timescale about 2–3 times larger. It is not clear why this discrepancy exists, but it is most probably due to the large differences between the relatively sharp time averaged density gradients in the POP model compared to the highly smoothed density gradients in the Levitus (1982) database used by Treguier et al. (1997).

Figure 6 shows the magnitude of the bolus velocity, $|K\boldsymbol{\nabla}h/\overline{h}|$, if β in (8) is simply replaced by β_e, where the effective beta is due to bottom topography as represented in the model. The pattern is scaled by a factor of 0.001 to make it comparable to the results of the model. The Richardson number is calculated by taking the vertical average of $(\partial_z\mathbf{u})^2/N^2$ over the top 1000 m of the model ocean, where both the numerator and denominator are time averages. This procedure neglects possible time correlations between the stratification and the vertical shear, but it appears to be the appropriate choice for a mesoscale parameterization, which is intended to apply to coarse resolution, steady state, or slowly evolving ocean circulation models. Taking the average of $(\partial_z\mathbf{u})^2/N^2$ over a uniform

depth of 1000 m does not allow for a thinner thermocline at the equator and probably leads to an overestimate of the Richardson number there. Our results show many of the features noted by Stammer (1998) on the basis of the Levitus et al. (1994) hydrographic data. This is not surprising as the POP model simulation does have the high energy regions in roughly the correct locations, although there is considerable drift away from the initial conditions for water mass structure. Note in Fig. 6 that the Held–Larichev closure predicts almost no bolus velocity in tropical regions and very little in coastal areas. Large bolus velocity is predicted in very compact regions in the western boundary current regions of the Northern Hemisphere. The main discrepancy with Fig. 4 is that Fig. 6 also predicts very high bolus velocity poleward of the Circumpolar Current and in the subpolar North Atlantic. There are two factors that cause this bias toward high latitudes. One is that the effective beta becomes smaller at high latitudes, and the other is that the weak stratification makes the timescale smaller in polar waters. A caveat in the interpretation of these results is that a different representation of the effective beta calculated from very high resolution bottom topography data might have an important impact on these results at high latitudes. In the model the depth is represented in terms of the discrete model-specified level depths. Thus, many areas are represented as flat, which may in reality have rough, but low amplitude, topography. Thus, the effective beta could be much higher than represented by the model.

VMHS have tested a number of parameterizations of mesoscale eddies by fitting detailed eddy resolving calculations with parameterized, zonally averaged models. Of all the parameterizations which they tested, they found the best results for a formulation called "NEW." This is composed of the GM parameterization for thickness mixing combined with a mixing coefficient similar to that proposed by Stone (1972) in a somewhat different context. For convenience, we will call NEW the VMHS–Stone parameterization. In this case the timescale of the mixing is the Eady timescale given by (6), and the length scale is either based on the geometry or, following Stone (1972), is taken to be proportional to the radius of deformation. As pointed out by Stammer (1998), a typical space scale of mesoscale eddies in the ocean would be expected to be about a factor of 3–4 times the radius of deformation. In this case, the mixing coefficient is simply

$$K_{\text{VMHS–Stone}} = \mu \frac{\lambda^2}{T}, \tag{10}$$

where λ is the radius of deformation and μ is a constant. The radius of deformation, $\lambda = NH/f$, is evaluated by averaging the stratification over the upper one kilometer of the water column, and taking H to have a constant value of one kilometer. Near the equator where the radius of deformation defined in this way exceeds the local distance to the equator, the equatorial radius of defor-

mation is used. The results are shown in Fig. 7. The improvement of fit to Fig. 4 compared to Figs. 5 and 6 is striking. This closure predicts bolus velocity at the equator in the eastern equatorial Pacific, in the Northern Hemisphere western boundary currents, and in the Antarctic Circumpolar Current. The high bolus velocities at polar latitudes predicted by the GM and HL closures are missing since the radius of deformation decreases so rapidly with respect to latitude. From a global perspective the closure given in (10) is clearly an improvement on those proposed initially by GM and HL.

Correlations of the patterns in Figs. 5–7 with the pattern in Figs. 4a,b are shown in Table 2. The correlations are calculated for a regression line, $y = mx$, constrained to pass through the origin

$$r^2 = \left(\sum xy \right)^2 \bigg/ \left(\sum x^2 \sum y^2 \right). \tag{11}$$

The correlations in all three cases are low, but they provide a quantitative confirmation of the visual impression of Figs. 4–7. The VMHS–Stone parameterization provides the highest correlation with the model bolus pattern followed by the original GM parameterization with a constant coefficient. Clearly, the use of the space-varying mixing coefficient in the VMHS–Stone case has a favorable impact in the Southern Ocean on the fit to the model bolus fields. The global pattern of the Stone mixing coefficient for the Los Alamos model is shown in Fig. 8. This smoothed field is computed by taking the ratio of the pattern in Fig. 7 and the pattern of the pure GM bolus magnitude shown in Fig. 5. Areas where the mixing coefficient exceeds 1000 m² s⁻¹ are the light regions along the western boundaries in the Northern Hemisphere and along the axis of the Circumpolar Current in the Southern Ocean. Generally, the coefficient is large where the magnitude of the bolus velocity shown in Fig. 4a is large, except at the equator. In Fig. 4a, bolus activity is generally confined to the eastern equatorial Pacific, but the Stone coefficient is large all along the equator.

4. Results for the absolute divergence

A basic assumption in the interpretation of the results of the previous section is that the rotational and diver-

TABLE 2. Correlation coefficients between the magnitude of the bolus velocity in the POP model shown in Fig. 4 and the parameterized magnitude of bolus velocities from the averaged model thickness fields shown in Figs. 5–7.

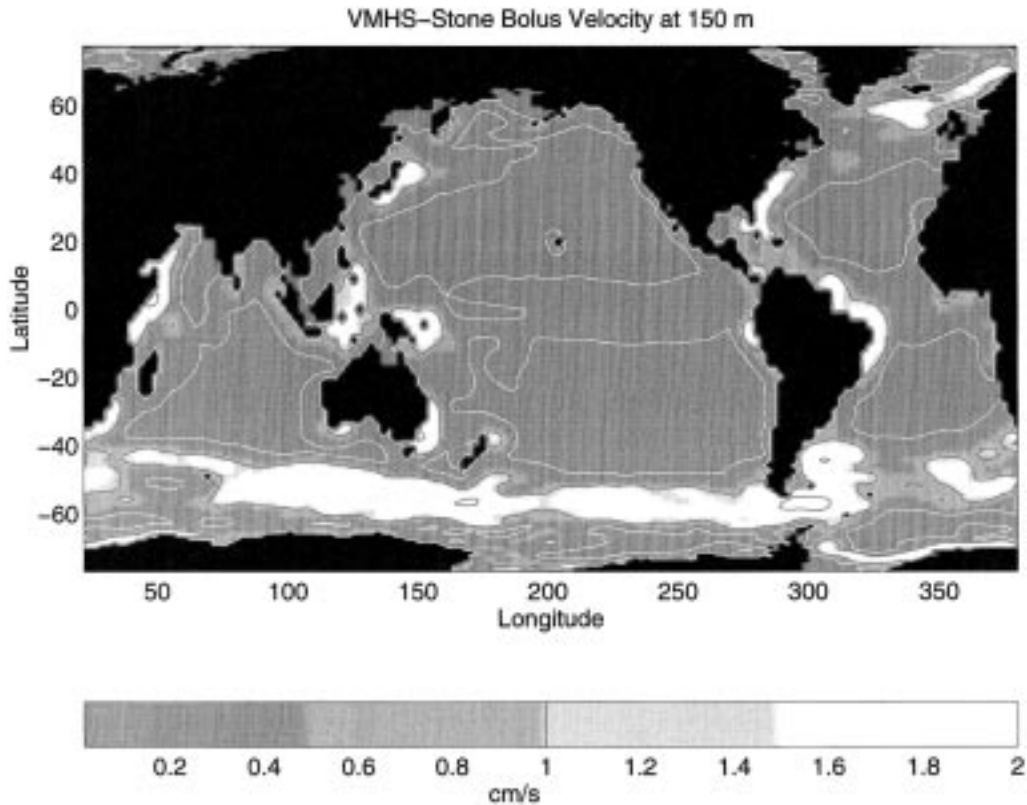| Level (m)		Global	Northern Hemisphere	Southern Hemisphere
150	GM	0.32	0.34	0.33
	HL	0.07	0.03	0.09
	VMHS	0.47	0.44	0.49
300	GM	0.37	0.39	0.40
	HL	0.11	0.04	0.14
	VMHS	0.46	0.49	0.47

FIG. 7. The magnitude of the bolus velocity predicted by the VMHS–Stone closure at the 150-m level. The GM mixing coefficient is proportional to the radius of deformation squared divided by the Eady timescale. A factor of 0.13 has been applied.

gent component of the bolus flux are sufficiently correlated on a global scale so that the magnitude of the bolus flux can be used as a proxy for the divergent component alone. To test this assumption we repeat some of the calculations using the field of the absolute value of the bolus flux divergence. We have used the absolute value because this allows spatial smoothing without the loss of amplitude, but eliminates the rotational component. The correlations of the absolute divergence of the bolus flux and the scalar bolus field are given in Table 3. Although these are very different quantities, the spatial patterns are correlated on a global scale.

Table 4 shows the correlations between the global patterns of the model and the predictions based on model thickness gradients of the GM and VMHS–Stone parameterizations. The results in Table 4 are calculated in the same way as in Tables 2 and 3. The correlations in Table 4 show nearly the same agreement between the model and the parameterizations as shown in Table 2 for the scalar bolus velocities. The correlations are too low to make a meaningful estimate of the regression line and the coefficient, μ, in (10). It is found that the least squares fit is very sensitive to extreme values, and the correlation and best fit regression coefficient increase as extreme values are discarded in the analysis. For purposes of displaying the parameterization patterns in Fig. 7 and Fig. 8, we have used a nominal coefficient, $\mu = 0.13$. This value is approximately equivalent to the "universal constant" $\mu = 0.015 \pm 0.005$ of VMHS since their mixing coefficient is based on a formula including the measured mixing scale in their numerical

TABLE 3. Correlation coefficients between the magnitude of the bolus velocity in the POP model shown in Fig. 4 and the magnitude of bolus flux divergence shown in Fig. 9. These correlations are calculated for a regression line constrained to pass through the origin.

Level (m)	Global	Northern Hemisphere	Southern Hemisphere
150	0.77	0.73	0.79
300	0.72	0.74	0.78

TABLE 4. Correlation coefficients between the magnitude of the bolus flux divergence in the POP model and the parameterized magnitude of bolus flux divergence.

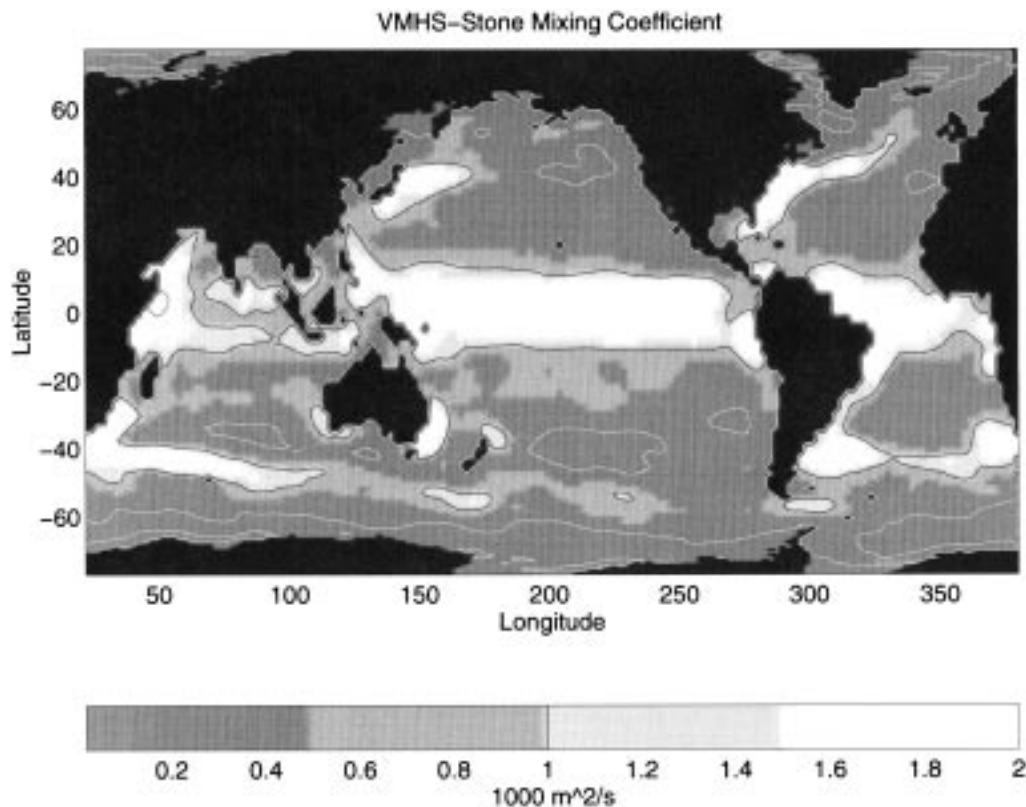| Level (m)		Global	Northern Hemisphere	Southern Hemisphere
150	GM	0.36	0.35	0.37
	VMHS	0.47	0.40	0.49
300	GM	0.39	0.44	0.38
	VMHS	0.49	0.49	0.47

FIG. 8. The VMHS–Stone mixing coefficient computed from the Los Alamos model. A constant of 0.13 is used. Contours are drawn for 100, 1000, and 10 000 m² s⁻¹.

experiments. Using Stammer's (1998) estimate that mesoscale eddies have a scale, which is approximately 3–4 times the radius of deformation, it is not unreasonable to expect that a coefficient μ an order of magnitude larger is required if the the radius of deformation is used as the mixing length scale.

The absolute value of the bolus flux divergence is plotted in Fig. 9. If we compare the pattern to the magnitude the bolus flux in Fig. 4a, we see many features in common. The amplitude is greatest in the areas where we expect mesoscale activity to exist, the vicinity of the Antarctic Circumpolar Current and the midlatitude region of the Northern Hemisphere oceans. However, there are significant differences in the details. It would be reasonable for the magnitude of the bolus velocity to be greater along the axis of jets, with the divergence stronger along the jet flanks. In the North Pacific sector of Fig. 9, the divergence does seem to be split by the jet axis. A major difference between Fig. 4a and Fig. 9 is at the equator. This suggests that the rotational component of the bolus velocity may dominate in this region. Care must be taken not to overinterpret details of the pattern in Fig. 9 because it is highly smoothed.

5. Summary and conclusions

The existence of statistics from a global ocean circulation model, which nearly resolves mesoscale eddies,

provides a unique opportunity to test proposed relationships between the large-scale time-averaged flow and mesoscale eddies. It appears that the rotational component of the bolus flux is comparable to the divergent component. This finding corresponds to that of Lau and Wallace (1979) who found that vorticity flux in atmospheric data also had a rotational and divergent component. Typically, the rotational component of the bolus velocity is overlooked or ignored in discussing parameterizations (Smith 1999). While it may play no role in the mean equations of motion and hence need not be parameterized, the existence of this rotational component introduces a complicating factor in the verification of parameterization schemes from model output or observations of eddy thickness fluxes.

An overall measure of bolus flux is simply the magnitude of the bolus velocity. Projections of the bolus velocity obtained by averaging on density surfaces are projected onto level surfaces at 150 and 300 m. This permits a global view that cannot be obtained by simply looking at density surfaces. The bolus patterns indicate maxima where eddy kinetic energy is known to be high from the observed variability of the sea surface elevation. In low latitudes, bolus velocity is large along the equator. In middle latitudes, there is high bolus velocity magnitude in the western boundary currents of the
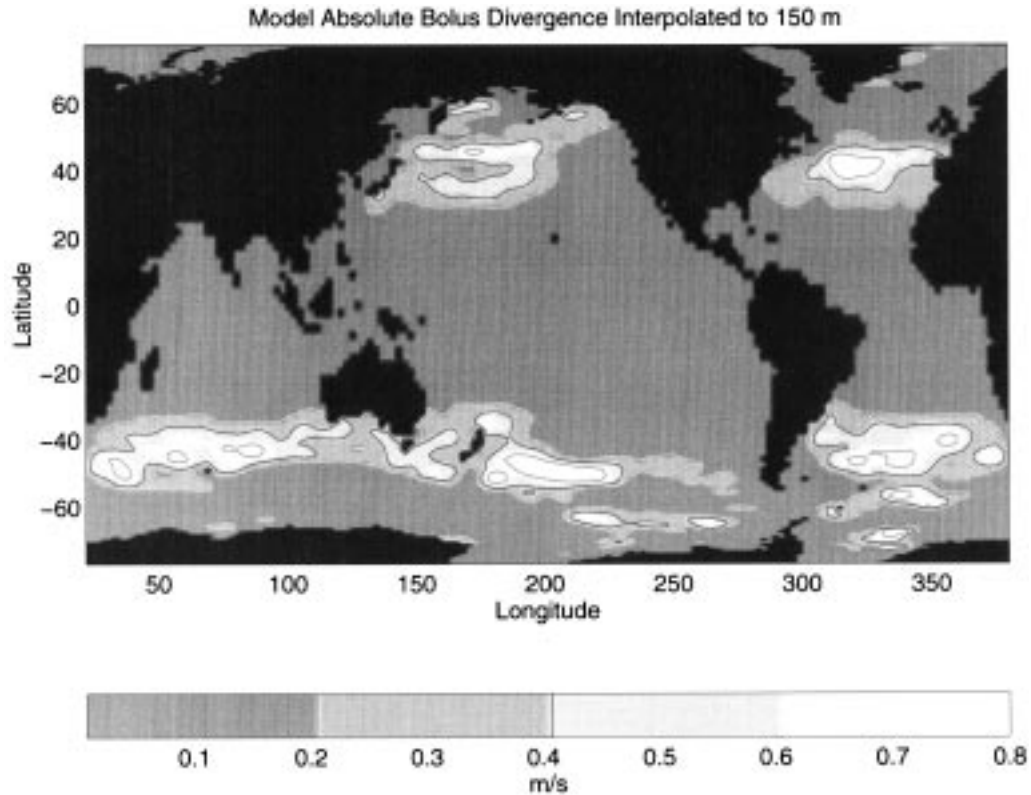
FIG. 9. The smoothed absolute value of the bolus divergence flux of the POP model interpolated to the 150-m level. The units are meters per second.

Northern Hemisphere and along the Antarctic Circumpolar Current in the Southern Hemisphere.

It was not possible to find simple relationships between the curl of the thickness flux and the divergence of the thickness flux in the 5-yr average of the POP ocean circulation model available for this study. While the magnitude of the bolus flux lumps both the rotational and divergent component together, it does provide a gross measure of bolus activity. The results show that the bolus magnitude appears to be adequate to discriminate between parameterizations, which have rather large qualitative differences. This conclusion is tested by a second approach in which the smoothed absolute value of the bolus flux divergence is also compared with the parameterizations. This second approach eliminates the contribution of the rotational component. Three different closures have been tested: 1) a constant coefficient designated as GM, 2) a diffusion coefficient suggested by HL, and 3) a diffusion coefficient suggested by VMHS. Many of our model results are anticipated by a complementary study of observational data carried out by Stammer (1998). Comparing with the bolus velocity magnitude predicted by the POP model, the closure suggested by VHMS–Stone appears to be superior, with the original GM parameterization a close second. We deliberately use the designation VHMS–Stone. While the mixing coefficient is essentially due to Stone, the ap-plication to thickness mixing was first suggested by VMHS. GM and HL both appear to overpredict the magnitude of the bolus flows in high latitude areas of weak stratification, while indicating little or no bolus activity near the equator. The VMHS–Stone diffusion coefficient used in this study is proportional to the square of the radius of deformation so that it predicts bolus activity along the equator, where the radius of deformation is large, and it greatly reduces the bolus activity at very high latitudes, where the radius of deformation is very small. This is the type of latitudinal dependence suggested by the scalar bolus velocity fields of the POP global circulation model.

Both the Held–Larichev parameterization and the VMHS–Stone parameterization depend on the Richardson number. Why is it then that the two methods give such different results? As pointed out by Stammer (1998) the difference is in the way the space scales are calculated. In the VMHS–Stone case the space scales are based on the radius of deformation, while in the HL formulation the Rhines length scale is used. The complex bottom topography of the World Ocean means the the Rhines scale will probably be quite small and difficult to estimate. The radius of deformation is much easier to calculate in a numerical model, and in any case, the Rhines scale may be nearly proportional to the radius of deformation. Thus the observed correspon-

TABLE A1. Position of levels in the POP Global Ocean circulation mode in meters.

	Level number									
	1	2	3	4	5	6	7	8	9	10
Layer thickness	25	25	25	25	35	50	75	100	150	200
Layer base depth	25	50	75	100	135	185	260	360	510	710
Level number	11	12	13	14	15	16	17	18	19	20
Layer thickness	275	350	415	450	550	550	550	550	400	400
Layer base depth	985	1335	1750	2200	2750	3300	3850	4400	4800	5200

dence between eddy length scales and the radius of deformation provides a more practical, empirical basis for a downgradient closure.

Although the visual correspondence of the bolus patterns of the POP simulations with the parameterized bolus patterns is suggestive, the actual statistical correlations are rather low. Thus, while the model data indicate the same ''universal'' constant as found by VMHS, the statistics only explain a small part of the variance. An important issue not included in our analysis is the role of eddies in the nonadiabatic regions near the ocean surface. The GM parameterization does not include regions of steep isopycnal slopes near the surface. Yet as suggested by Tandon and Garrett (1996) and Treguier et al. (1997) mixing by mesoscale eddies in such regions can be very important. The analysis of surface mixing should be included in future studies of mesoscale eddy-permitting models. In the future it may be possible to design global ocean circulations specifically for investigating mesoscale eddy parameterizations. The greatest uncertainties in the present study center around the resolution of the model, discretization errors in the vertical, and statistical uncertainty connected with the length of the averaging period. This suggests that future studies should be carried out with ocean circulation models of much higher horizontal resolution, possibly using isopycnal coordinates, generating statistics from much longer time series.

APPENDIX

Details of the POP World Ocean Model

This appendix is intended to summarize material given in Fu and Smith (1996) and Maltrud et al. (1998) needed to provide some background on the POP global model. The model has 20 levels whose spacing is given in Table A1 below. The horizontal grid is based on a Mercator projection extending from 77°S to 77°N. Grid points are placed 0.28 of a degree apart at the equator. The Mercator projection provides double the resolution at 60° latitude, where the shrinking radius of deformation makes mesoscale eddies more difficult to resolve. The model uses biharmonic viscosity and diffusion in the horizontal plane with the coefficients varying with the cube of the horizontal grid spacing. Let η and κ be the biharmonic coefficients for lateral viscosity and diffusivity, respectively,

$$(\eta, \kappa) = -(6, 2) \times 10^{19} \cos^3 \varphi \quad [\text{cm}^4 \text{ s}^{-1}]. \quad (A1)$$

The Pacanowski and Philander (1981) scheme was used for representing vertical viscosity and diffusion, with background values 1.0 and 0.1 cm^2 s^{-1}, respectively. The initial values for Stage I of the model are based on values of temperature and salinity given by a 32 year run with a ½ degree model followed by 3-year run with a ¼ degree model. Details of the forcing are given in Table A2 taken from Maltrud et al. (1998). During the entire spin up of the model and in all subsequent experiments, salinity is restored to the seasonal Levitus (1982) climatology. Surface temperatures are forced in the same way in the early phase, but for the final stage of the run the temperature is forced by the Barnier et al. (1995) heat fluxes, with a feedback to prevent the surface temperature from drifting too far from obser-

TABLE A2. Surface forcing during the spinup of the POP Global Ocean circulation model. Winds are based on ECMWF analyses. Levitus damping refers to a damping of the surface layer to the season surface climatology given in the Levitus (1982) dataset. Initial values for stage I are based on Semtner (1998).

	Stage		
	I	II	III
Duration	Jan 1985–Jun 1993	Jan 1985–May 1994	Mar 1985–Dec 1995
Years	8.5	9.42	10.75
Wind frequency	Monthly	3-day	3-day
Surface salinity	Levitus damping	Levitus damping	Levitus damping
Surface temperature	Levitus damping	Levitus damping	Barnier flux

vations. This feedback may be relatively large in the case of strong currents near coastlines.

REFERENCES

Barnier, B., L. Siefridt, and P. Marchcsiello, 1995: Thermal forcing for a global ocean circulation model using a three-year climatology of ECMWF analyses. *J. Mar. Syst.,* **6,** 363–380.

Böning, C. W., and P. Herrmann, 1994: Annual cycle of poleward heat transport in the ocean: Results from high-resolution modeling of the north and equatorial Atlantic. *J. Phys. Oceanogr.,* **24,** 91–107.

——, R. Holland, F. Bryan, G. Danabasoglu, and J. C. McWilliams, 1995: An overlooked problem in model simulations of the thermohaline circulation and heat transport in the Atlantic Ocean. *J. Climate,* **8,** 515–523.

Cox, M. D., 1987: Isopycnal diffusion in a *z*-coordinate ocean model. *Ocean Modelling* (unpublished manuscripts), **74,** 1–5.

Danabasoglu, G., and J. C. McWilliams, 1995: Sensitivity of the global ocean circulation to parameterizations of mesoscale tracer transports. *J. Climate,* **8,** 2967–2987.

——, ——, and P. R. Gent, 1994: The role of mesoscale tracer transports in the global ocean circulation. *Science,* **264,** 1123–1126.

Eady, E. T., 1949: Long waves and cyclone waves. *Tellus,* **1,** 33–52.

Fu, L.-L., and R. D. Smith, 1996: Global ocean circulation from satellite altimetry and high resolution computer simulation. *Bull. Amer. Meteor. Soc.,* **77,** 2625–2636.

Gent, P. R., and J. C. McWilliams, 1990: Isopycnic mixing in ocean circulation models. *J. Phys. Oceanogr.,* **20,** 150–155.

Green, J. S., 1970: Transfer properties of the large-scale eddies and the general circulation of the atmosphere. *Quart. J. Roy. Meteor. Soc.,* **96,** 157–185.

Held, I. M., and V. D. Larichev, 1996: A scaling theory for horizontally homogeneous, baroclinically unstable flow on a beta plane. *J. Atmos. Sci.,* **53,** 946–952.

Lau, N.-C., and J. M. Wallace, 1979: On the distribution of horizontal transports by transient eddies in the Northern Hemisphere wintertime circulation. *J. Atmos. Sci.,* **36,** 1844–1861.

Levitus, S., 1982: *Climatological Atlas of the World Ocean.* NOAA Prof. Paper No. 13, U.S. Dept. of Commerce, 174 pp.

——, R. Burgett, and T. Boyer, 1994: *World Ocean Atlas, 1994,* Vol. 3: *Salinity*; Vol. 4: *Temperature,* NOAA Atlas NESDIS 3; 4, US. Dept. Commerce, 117 pp; 99 pp.

Maltrud, M. E., R. D. Smith, A. J. Semtner, and R. C. Malone, 1998: Global eddy-resolving ocean simulations driven by 1985–1994 atmospheric winds. *J. Geophys. Res.,* **103** (C13), 30 825–30 853.

Marshall, J. C., and G. Shutts, 1981: A note on rotational and divergent eddy fluxes. *J. Phys. Oceanogr.,* **11,** 1677–1680.

McDougall, T., and P. McIntosh, 1996: The temporal-residual-mean velocity. Part I: Derivation and the scalar conservation equations. *J. Phys. Oceanogr.,* **26,** 2653–2665.

Pacanowski, R. C., and S. G. H. Philander, 1981: Parameterization of vertical mixing in numerical models of tropical oceans. *J. Phys. Oceanogr.,* **11,** 1443–1451.

Redi, M. H., 1982: Oceanic mixing by coordinate rotation. *J. Phys. Oceanogr.,* **12,** 87–94.

Reid, J. L., and R. J. Lynn, 1971: On the influence of the Norwegian–Greenland and Weddell seas upon the bottom waters of the Indian and Pacific oceans. *Deep-Sea Res.,* **18,** 1063–1088.

Rhines, P. B., 1975: Waves and turbulence on a beta-plane. *J. Fluid Mech.,* **69,** 417–443.

Rix, N. H., and J. Willebrand, 1996: Parameterization of mesoscale eddies as inferred from a high-resolution circulation model. *J. Phys. Oceanogr.,* **26,** 2281–2285.

Smith, R. D., 1999: The primitive equations in the stochastic theory of adiabatic stratified turbulence. *J. Phys. Oceanogr.,* **29,** 1865–1880.

Stammer, D., 1998: On eddy characteristics, eddy transports, and mean flow properties. *J. Phys. Oceanogr.,* **28,** 727–739.

Stone, P. H., 1972: A simplified radiative–dynamical model for the static stability of rotating atmospheres. *J. Atmos. Sci.,* **29,** 405–418.

Tandon, A., and C. Garrett, 1996: On recent parameterization of mesoscale eddies. *J. Phys. Oceanogr.,* **26,** 406–411.

Treguier, A. M., I. M. Held, and V. D. Larichev, 1997: On the parameterization of quasi-geostrophic eddies in primitive equation ocean models. *J. Phys. Oceanogr.,* **27,** 567–580.

Veronis, G., 1975: The role of models in tracer studies. *Numerical Models of Ocean Circulation,* Natl. Acad. Sci., 133–146.

Visbeck, M., J. Marshall, T. Haine, and M. Spall, 1997: On the specification of eddy transfer coefficients in coarse resolution ocean circulation models. *J. Phys. Oceanogr.,* **27,** 381–402.